THE JOURNAL OF BIOLOGICAL CHEMISTRY VOL. 287, NO. 43, pp. 36341–36355, October 19, 2012

Mechanism and Significance of Changes in Glutamate-Cysteine Ligase Expression during Hepatic Fibrogenesis*[S]

Received for publication, April 10, 2012, and in revised form, August 21, 2012 Published, JBC Papers in Press, August 31, 2012, DOI 10.1074/jbc.M112.370775

Komal Ramani[1], **Maria Lauda Tomasi**[1], **Heping Yang, Kwangsuk Ko**[2], **and Shelly C. Lu**[3]

From the Division of Gastroenterology and Liver Diseases, USC Research Center for Liver Diseases, Southern California Research Center for Alcoholic and Pancreatic Diseases and Cirrhosis, Keck School of Medicine of University of Southern California, Los Angeles, California 90033

Background: GSH defends against oxidative stress, which activates hepatic stellate cells (HSCs).
Results: A high GSH level keeps HSCs in a quiescent state, and this requires sumoylation of Nrf2 and MafG, which facilitates heterodimerization and activation of the antioxidant response element (ARE).
Conclusion: GSH is an important determinant of the HSC phenotype.
Significance: This is the first report of Nrf2 and MafG sumoylation driving ARE-dependent gene expression in HSCs.

GSH is synthesized sequentially by glutamate-cysteine ligase (GCL) and GSH synthase and defends against oxidative stress, which promotes hepatic stellate cell (HSC) activation. Changes in GSH synthesis during HSC activation are poorly characterized. Here, we examined the expression of GSH synthetic enzymes in rat HSC activation and reversion to quiescence. Expression of the GCL catalytic subunit (GCLC) fell during HSC activation and increased when activated HSCs revert back to quiescence. Blocking the increase in GCLC expression kept HSCs in an activated state. Activated HSCs have higher nuclear levels and binding activity of MafG to the antioxidant response element (ARE) of GCLC but lower Nrf2/MafG heterodimer binding to the ARE. Quiescent HSCs have a lower nuclear MafG level but higher Nrf2/MafG heterodimer binding to ARE. This occurred because of enhanced sumoylation of Nrf2 and MafG by SUMO-1, which promoted Nrf2 binding to ARE and heterodimerization with MafG. *In vivo*, knockdown of GCLC exacerbated bile duct ligation-induced liver injury and fibrosis. Ursodeoxycholic acid and *S*-adenosylmethionine are anti-fibrotic in bile duct ligation, but this effect was nearly lost if GCLC induction was blocked. In conclusion, sumoylation of Nrf2 and MafG enhances heterodimerization and increases GCLC expression, which keeps HSCs in a quiescent state. Antifibrotic agents require activation of GCLC to fully exert their protective effect.

GSH is a tripeptide that is sequentially synthesized in all mammalian cells via two enzymatic steps as follows: the formation of γ-glutamylcysteine from glutamate and cysteine catalyzed by glutamate-cysteine ligase (GCL)[4]; and the formation of GSH from γ-glutamylcysteine and glycine catalyzed by GSH synthase (GS) (1). GCL is the rate-limiting enzyme that is made up of two subunits, the catalytic (GCLC) and the modifier (GCLM) subunits (1). GSH protects against oxidative stress and regulates many important cellular events, including fibrogenesis (1). Hepatic stellate cells (HSCs) play a central role in fibrogenesis. Following chronic liver injury, HSCs proliferate, lose their vitamin A, and undergo a major phenotypical transformation (transdifferentiation or activation) to α-smooth muscle actin (α-SMA)-positive activated HSCs, which produce a wide variety of collagenous and noncollagenous extracellular matrix proteins and components that inhibit fibrosis degradation (2). Activation of HSC is mediated by various cytokines and reactive oxygen species released from damaged hepatocytes and activated Kupffer cells (3). Several reports implicated the importance of GSH in fibrogenesis. Profibrogenic factor TGF-β1 suppressed the expression of GCLC and lowered GSH levels in rat HSCs (4). Epigallocatechin-3-gallate, the major constituent of green tea, blocked the effect of TGF-β1 on GCLC expression and HSC activation (4). Similarly, curcumin also blocked HSC activation by raising GSH levels (5). Despite these reports, changes in expression of GSH synthetic enzymes and GSH levels during fibrogenesis remain poorly characterized.

We reported hepatic expression of GCL subunits, and GS decreased markedly along with GSH levels during later stages of bile duct ligation (BDL) in mice, which is a model of cholestatic liver injury and fibrosis (6). This was associated with displacement of nuclear factor-erythroid 2-related factor 2 (Nrf2) nuclear binding to the antioxidant response element (ARE), which is present in the promoter region of many genes involved

* This work was supported, in whole or in part, by National Institutes of Health Grants K99AA017774 (to K. R.), R01DK092407 and R01AT1576 (to S. C. L. and H. Y.), and F32AA020150 (to M. L. T.).
[S] This article contains supplemental Fig. 1 and an additional reference.
The nucleotide sequence(s) reported in this paper has been submitted to the GenBank™/EBI Data Bank with accession number(s)AY382195
[1] Both authors contributed equally to this work.
[2] Present address: Dept. of Nutritional Science and Food Management, the College of Health Science, Ewha Womans University, Seoul 120-750, Korea.
[3] To whom correspondence should be addressed: Keck School of Medicine USC, HMR 415, 2011 Zonal Ave., Los Angeles, CA 90033. Tel.: 323-442-2441; Fax: 323-442-3234; E-mail: shellylu@usc.edu.

[4] The abbreviations used are: GCL, glutamate-cysteine ligase; α-SMA, α-smooth muscle actin; ALT, alanine transaminase; ARE, antioxidant response element; BDL, bile duct ligation; BSC, biliary fibrosis-derived stellate cell; Col1A2, collagen α2(I); GCLC, GCL-catalytic subunit; GCLM, GCL-modifier subunit; GS, GSH synthase; HSC, hepatic stellate cell; Nrf2, nuclear factor-erythroid 2 related factor 2; PPARγ, peroxisome proliferator-activated receptor γ; AdoMet, *S*-adenosylmethionine; SeqChIP, sequential ChIP; SUMO-1, ubiquitin-related modifier-1; UDCA, ursodeoxycholic acid.

in antioxidant defense, including GSH synthetic enzymes (1, 6). In subsequent work, we demonstrated that Nrf2 displacement from ARE binding was likely due to an increase in the hepatic expression of c-Maf and MafG (7). These Maf proteins have the capability to negatively regulate ARE-mediated gene expression as knocking down c-Maf and MafG protected against the fall in Nrf2 binding to ARE and expression of GSH synthetic enzymes (7). In the BDL model, ursodeoxycholic acid (UDCA) and *S*-adenosylmethionine (AdoMet), the main cellular methyl donor that is also a precursor for hepatic GSH (8), exerted a protective effect against BDL-induced liver injury and fibrosis (6). These agents were able to prevent the induction in c-Maf and MafG expression, displacement of Nrf2 from ARE nuclear binding, and the fall in hepatic expression of GSH enzymes (7). Because these studies examined changes in the whole liver, which is composed of mostly hepatocytes, whether GSH synthetic enzymes are also down-regulated in HSCs during fibrogenesis remains unknown.

The aims of the this study were to examine whether the expression of GSH synthetic enzymes changes during HSC activation and to assess the role of GCLC expression and GSH level in determining HSC phenotype and treatment efficacy of UDCA and AdoMet. Our results indicate a vital role of GCLC expression as a determinant of HSC phenotype and as a key target of anti-fibrotic agents to exert their full therapeutic effect. We also uncovered a novel post-translational modification that is required for Nrf2/MafG heterodimerization and binding to the ARE. Interestingly, in quiescent HSCs, heterodimerization with Nrf2 is markedly enhanced despite much lower nuclear MafG levels. This is due to increased sumoylation of Nrf2 and MafG, which has not been reported previously to facilitate Nrf2/MafG interaction and *trans*-activation of ARE.

EXPERIMENTAL PROCEDURES

Materials—UDCA was obtained from Sigma. AdoMet in the form of disulfate *p*-toluenesulfonate dried powder was generously provided by Gnosis SRL (Cairate, Italy). [α-^{32}P]dCTP (3,000 Ci/mmol) was purchased from PerkinElmer Life Sciences. All other reagents were of analytical grade and obtained from commercial sources.

Animal Use—The Institutional Animal Care and Use Committee of the University of Southern California approved all animal usage in this study. HSCs were isolated from normal male Wistar rats or 10-day-old BDL rats by the Non-Parenchymal Liver Cell Core of the Research Center for Alcoholic Liver and Pancreatic Diseases and Cirrhosis as described previously (9). The purity of isolated HSCs was examined by ultraviolet-excited fluorescence microscopy, and viability was determined by trypan blue exclusion. BDL and sham surgery were performed in 3-month-old male C57BL/6 mice as we described (6). In some experiments, under the same anesthesia for sham surgery or BDL, mice also received GCLC siRNA or scrambled control (1×10^9 transducing units in 0.1 ml injected into the spleen) as we described (7). The shRNA pre-made lentivirus GCLC (catalog no. RMM4532-NM_010295), empty lentivirus (catalog no. RHS4349) vectors, packaging plasmid, Trans-Lentiviral pGIPZ Packaging System (catalog no. TLP4614), and envelope plasmid were purchased from Open Biosystems (Huntsville, AL), and viral harvesting was done as described in the protocol. Second and 3rd injections on days 6 and 10 were performed through the tail vein. On days 3, 7, 10, and 14 post-surgery, hepatocytes were isolated to assess transduction efficiency using GFP, which is included in the lentivirus vector, as we described (7). To assess the effect of UDCA and AdoMet in the setting of GCLC knockdown, BDL mice treated with scrambled siRNA or GCLC siRNA also received either UDCA (100 mg/kg/day in 0.1 ml of 2.5% sodium bicarbonate, pH 7.4), AdoMet (100 mg/kg/day in 0.1 ml of Tris buffer, pH 7.4), both agents, or vehicle control by gavage as we described (6). Mice were sacrificed 14 days post-surgery, and sera and livers were harvested for studies described below.

HSC Activation and Differentiation Models—In vitro culture activation used normal rat HSCs cultured in low glucose DMEM supplemented with 10% FBS and antibiotics for 1, 3, 5, or 7 days. For *in vivo* activation, HSCs were isolated from 10-day-old BDL and sham-operated rats and cultured for 16 h in low glucose DMEM with 3% FBS before analysis. Biliary fibrosis-derived stellate cell (BSC) line is a spontaneously immortalized activated rat HSC cell line originally isolated from 18-day-old BDL rats (10), and cells were cultured in DMEM plus 10% FBS. Both cultured activated primary HSCs and BSCs can be reverted back to differentiated phenotypes by treatment with the adipogenic mixture MDI (0.5 mM methylisobutylxanthine, 1 μM dexamethasone, and 1 μM insulin) for 3 days as described (11).

To evaluate the role of GCLC, c-Maf, MafG, and SUMO-1 in HSC activation, BSCs were treated with double-stranded GCLC, MafG, c-Maf, small ubiquitin-related modifier-1 (SUMO-1), or scrambled siRNA. GCLC siRNA (catalog no. SI02780498, Qiagen), MafG siRNA (catalog no. sc-38099), c-Maf siRNA (catalog no. sc-38111), and SUMO-1 siRNA (catalog no. sc-156144) were purchased from Santa Cruz Biotechnology (Santa Cruz, CA). BSCs treated with or without MDI for 3 days were transfected with GCLC, MafG, c-Maf, SUMO-1, or scrambled siRNA (10 nM per 1×10^5 cells) using Lipofectamine™ RNAiMAX transfection reagent (Invitrogen). Transfection was done in 6-well plates at 30% confluency for 48 h either alone or during the last 2 days of the MDI treatment and were then processed for Western blot analysis and GSH level determination as described below.

Necrosis, Apoptosis, and Fibrosis Determination in Liver Specimens—Liver tissues were formalin-fixed, cut, and stained with H&E, and the percentage of necrosis was estimated by counting the number of microscopic fields with necrosis compared with the entire section in 15 different sections at ×100 magnification. Apoptosis was determined by staining with TUNEL according to the manufacturer's suggested protocol (*in situ* cell death detection kit, Roche Applied Science). Five random fields containing an average of 250 nuclei were counted for each TUNEL-stained tissue sample. The apoptotic index (percentage of apoptotic nuclei) of hepatocytes was calculated as (apoptotic nuclei/total nuclei) × 100%. Samples from at least three mice per treatment condition were scored. Fibrosis was determined by staining with 0.1% Sirius red (Sigma), quantified using a computer-assisted image analysis system (MetaMorph

imaging system; Universal Imaging Corp., Downingtown, PA), and expressed as stained area per total examined area.

RNA Isolation and Gene Expression Analysis—Total RNA was isolated by the TRIzol reagent (Invitrogen) from liver tissues or cells. Northern blot analyses for GCLC and collagen α2(I) (Col1A2) were done as we described (6). Specific GCLC, Col1A2, and β-actin probes were labeled with [^{32}P]dCTP using a random primer kit (RediPrime DNA Labeling System; Amersham Biosciences), and the results of Northern blot analysis were normalized to β-actin. Gene expression was also assessed using real time PCR. Total RNA was subjected to RT by using Moloney murine leukemia virus reverse transcriptase (Invitrogen). Two μl of RT product was subjected to real time PCR analysis. The primers and TaqMan probes for rat GCLC, GCLM, GS, peroxisome proliferator-activated receptor γ (PPARγ), α-SMA, and the Universal PCR Master Mix were purchased from ABI (Foster City, CA). Hypoxanthine phosphoribosyltransferase 1 (HPRT1) was used as housekeeping gene. The thermal profile consisted of initial denaturation at 95 °C for 15 min followed by 40 cycles at 95 °C for 15 s and at 60 °C for 1 min. The cycle threshold (*Ct* value) of the target genes was normalized to that of HPRT1 to obtain the Δ*Ct*. The Δ*Ct* was used to find the relative expression of target genes according to the following formula: relative expression $= 2^{-\Delta\Delta Ct}$, where ΔΔ*Ct* = Δ*Ct* of target genes in experimental condition − Δ*Ct* of target gene under control conditions.

Western Blot and Immunoprecipitation Analysis—Total cellular protein from primary HSCs or BSCs was extracted following standard protocols (Amersham Biosciences) and resolved on 12% SDS-polyacrylamide gels. Western blotting was performed using primary antibodies as follows: GCLC, GCLM, and GS (Aviva Systems Biology, San Diego); PPARγ, Nrf2, MafG, and c-Maf (Santa Cruz Biotechnology); α-SMA (Abcam, Cambridge, MA); c-Myc, ubiquitin, and histone H3 (Santa Cruz Biotechnology); β-actin (Sigma); and HRP-conjugated secondary antibodies. Membranes were developed by chemiluminescence using the ECL detection system (Amersham Biosciences). Quantitation of blots was done using the Quantity One™ densitometry program (Bio-Rad). For immunoprecipitation, nuclear extracts were prepared using the EpiQuik nuclear extraction kit (Epigentek, Farmingdale, NY). Nuclear extracts were immunoprecipitated with antibodies against Nrf2, SUMO-1 (Abgent Inc., San Diego), or SUMO-2/3 (Santa Cruz Biotechnology) as described previously (12). Immunoprecipitated proteins were subjected to Western blotting using antibodies against MafG, Nrf2, c-Myc, and ubiquitin.

ChIP and Sequential ChIP (SeqChIP) Assay—To examine changes in protein binding to the ARE of the rat GCLC promoter in an endogenous chromatin configuration, ChIP assay was carried out following the ChampionChIP™ kit protocol (SABioscences, Frederick, MD). This kit was also used for the SeqChIP assay (13) to study co-localization of two proteins on the same region of the GCLC promoter. Briefly, DNA immunoprecipitated by Nrf2 antibody was processed for a second round of immunoprecipitation using anti-MafG antibody. The purified DNA was detected by PCR analysis. Antibodies used for SeqChIP were anti-Nrf2 and MafG (Santa Cruz Biotechnology). PCRs of the rat GCLC promoter region across ARE (GCGCTGAGTCAC, −3708/−3697 bp relative to ATG start site) (GenBank™ accession number AY382195) used forward primer 5′-TCCTTGGAGGCCCGAAACCCATC-3′ (bp −3853 to −3831) and reverse primer 5′-ACCGCCTCCCCGTGACTC-AGC-3′ (bp −3706 to −3686). All PCR products were run on 8% acrylamide gels and stained with ethidium bromide for 15–30 min.

Site-directed Mutagenesis of Nrf2 and MafG SUMO-1-binding Sites and Expression in BSC Cells—Rat Nrf2 and MafG expression vectors containing the full-length cDNA were purchased from Open Biosystems (Lafayette, CO). SUMO-1 consensus site mutants for Nrf2 and MafG were generated by Mutagenex Inc. (Hillsborough, NJ), and mutants were verified by sequencing. Mutated peptides are shown in supplemental Fig. 1. BSC cells were plated in 10-cm dishes (0.3×10^6 cells per dish) and transfected for 72 h with Nrf2 and MafG constructs using the Superfect transfection reagent (Qiagen).

GSH Levels—GSH levels in liver tissues and HSCs were measured as described previously (14).

Serum Alkaline Phosphatase, Bilirubin, and Alanine Transaminase (ALT) Levels—Serum alkaline phosphatase, bilirubin (Thermo Electron Corp., Waltham, MA), and ALT (RAICHEM, San Marcos, CA) levels were measured following the manufacturers' instructions.

Statistical Analysis—Data are given as means ± S.E. Statistical analysis was performed using analysis of variance followed by Fisher's test for multiple comparisons. For changes in mRNA and protein levels, ratios of the densitometric values of genes or proteins to respective housekeeping genes or proteins were compared. Significance was defined by $p < 0.05$.

RESULTS

Changes in the Expression of GSH Synthetic Enzymes during in Vitro and in Vivo HSC Activation—We first examined expression of GSH synthetic enzymes in primary HSCs activated during *in vitro* culture. Fig. 1*A* shows that both GCLC and GCLM mRNA levels decreased by day 3 and remained 60% reduced up to day 7. GS mRNA level was unchanged at day 3, but by day 5 it also fell by 50% and remained reduced at day 7. GSH levels fell significantly by day 5 and continued to fall to 30% of base line by day 7 (Fig. 1*B*). In HSCs isolated from 10-day-old BDL rats, the mRNA levels of GCLC and GCLM were also reduced by 50–60%, but the mRNA level of GS was unchanged (Fig. 1*C*). GSH levels in HSCs from BDL rats were 36% of sham HSC controls (Fig. 1*D*). Reduced GCLC expression was confirmed at the protein level by a comparable amount, whereas the GCLM protein level was not significantly changed (Fig. 1*E*). Note that GCLC is present as both 73-kDa and cleaved 60-kDa bands in HSCs from sham operated rats, and *in vivo* activation led to a fall in only the 73-kDa band.

GCLC Expression and GSH Level in a Model of Reversible HSC Activation—Activated HSCs revert back to quiescence following treatment with the adipogenic mixture MDI (11). Fig. 2 (*A* and *B*) shows that following MDI treatment in BSCs, α-SMA expression fell while PPARγ expression increased, and these are changes known to be associated with HSC differentiation. MDI treatment increased GCLC expression at both the mRNA and protein levels. Interestingly, MDI treatment lowered the 60-kDa cleaved GCLC band by 47%,

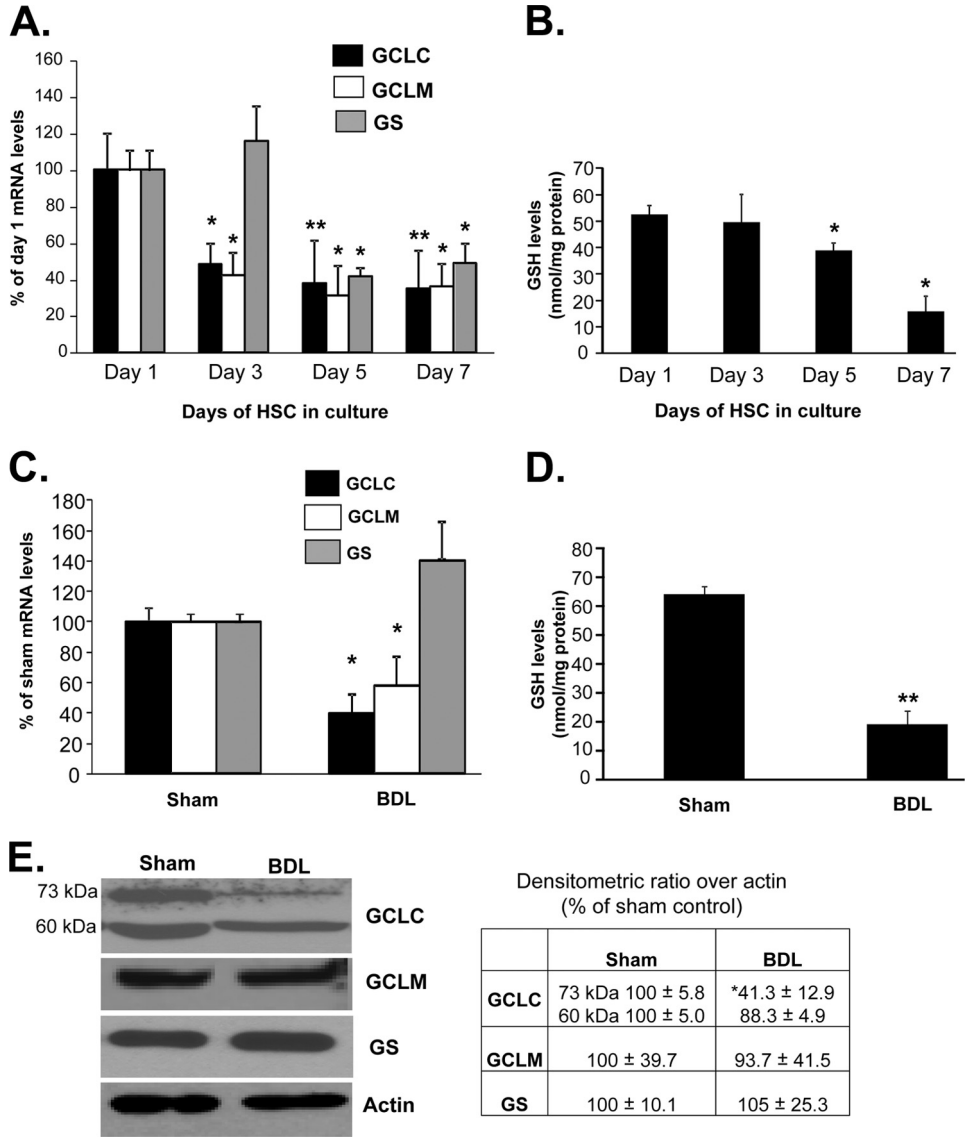

	Sham	BDL
GCLC	73 kDa 100 ± 5.8 60 kDa 100 ± 5.0	*41.3 ± 12.9 88.3 ± 4.9
GCLM	100 ± 39.7	93.7 ± 41.5
GS	100 ± 10.1	105 ± 25.3

FIGURE 1. **Changes in expression of GSH synthetic enzymes and GSH levels during HSC activation.** *A* shows changes in the mRNA levels of GCLC, GCLM, and GS during *in vitro* HSC activation measured by real time PCR. Results are expressed as mean ± S.E. from six primary HSC preparations. *, $p < 0.05$; **, $p < 0.005$ *versus* day 1. *B* shows changes in GSH levels during *in vitro* HSC activation. Results from two HSC preparations in duplicate for each time point are expressed as nanomoles of total GSH per mg of protein, *, $p < 0.05$ *versus* day 1. *C* shows changes in the mRNA levels of GCL subunits and GS during *in vivo* HSC activation measured by real time PCR from 10-day-old BDL or sham control HSCs. Results are from five preparations. *, $p < 0.05$ *versus* sham control. *D* shows changes in GSH levels during BDL-mediated HSC activation. Results are from two preparations in triplicate expressed as nanomoles of total GSH per mg of protein. **, $p < 0.005$ *versus* sham. *E* shows changes in the protein levels of GCL subunits and GS during *in vivo* HSC activation measured by Western blotting from 10-day-old BDL or sham control HSCs. Results are from two HSC preparations in duplicate. The *table* in *E* summarizes densitometric changes in the Western blots. *, $p < 0.05$ *versus* sham control.

and it more than doubled the 73-kDa band (Fig. 2*B*). However, we have observed inconsistencies in the appearance of the 60-kDa band in different preparations of MDI-treated BSC cells. The reason for this inconsistency is not known. Similar changes were also observed following treatment of culture-activated primary HSCs with MDI (Fig. 2, *C* and *D*). Intracellular GSH levels increased to 317 ± 22 and 192 ± 5% of control in BSCs and primary rat HSCs, respectively, following MDI treatment ($p < 0.005$ *versus* control from seven experiments in duplicate for BSCs and two primary HSC preparations in duplicate).

Effect of GCLC Knockdown on HSC Phenotype—To evaluate the importance of GCLC expression as a determinant of the HSC phenotype, BSCs were treated with GCLC siRNA or scrambled siRNA during the last 48 h of MDI treatment. Fig. 3 shows that when GCLC mRNA level is reduced by 50%, there is a significant increase in the expression of α-SMA (Fig. 3, *A* and *C*). Preventing GCLC induction during MDI treatment kept α-SMA expression elevated and blunted the PPARγ response (Fig. 3, *B* and *C*).

Nuclear Nrf2, c-Maf, and MafG Levels and Binding to GCLC ARE during HSC Activation and Reversion to Quiescent State—Nuclear Nrf2 levels in HSCs were not significantly altered after 10 days of BDL (Fig. 4*A*) or by MDI treatment in BSCs (Fig. 4*B*). However, both c-Maf and MafG nuclear levels increased during *in vivo* activation (Fig. 4*A*) and decreased following MDI treatment (Fig. 4*B*). Nuclear binding activity to ARE of rat GCLC promoter was evaluated by ChIP, and although nuclear Nrf2 levels

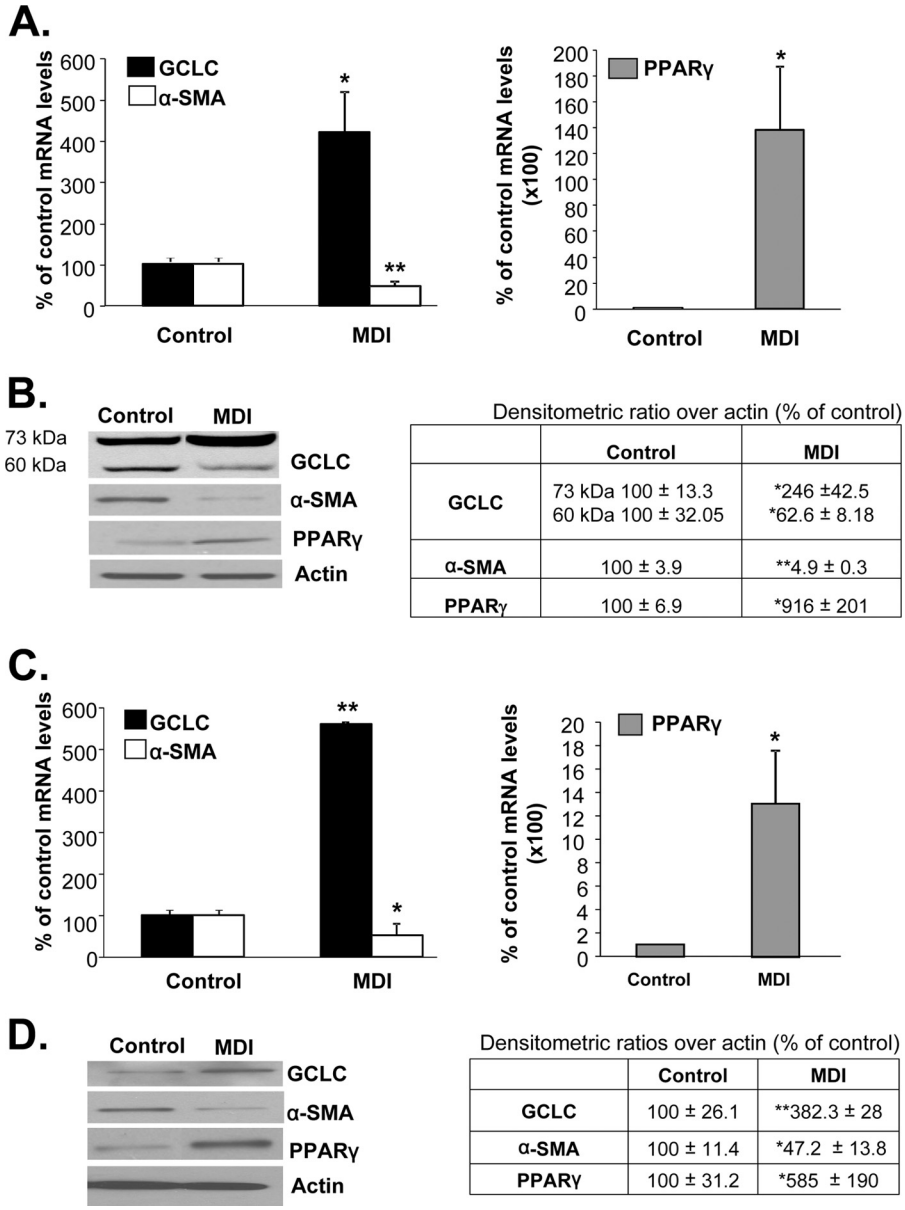

	Control	MDI
GCLC	73 kDa 100 ± 13.3 60 kDa 100 ± 32.05	*246 ±42.5 *62.6 ± 8.18
α-SMA	100 ± 3.9	**4.9 ± 0.3
PPARγ	100 ± 6.9	*916 ± 201

Densitometric ratios over actin (% of control)

	Control	MDI
GCLC	100 ± 26.1	**382.3 ± 28
α-SMA	100 ± 11.4	*47.2 ± 13.8
PPARγ	100 ± 31.2	*585 ± 190

FIGURE 2. **GCLC expression is increased when activated HSCs revert back to quiescence.** *A* and *B* show changes in mRNA (*A*) and protein (*B*) levels of GCLC, α-SMA, and PPARγ following MDI treatment of BSCs, which are activated at base line. The *table* in *B* summarizes densitometric changes in the Western blots. Results are from six experiments for mRNA, and three experiments were done in duplicate for protein levels. *, $p < 0.05$, and **, $p < 0.005$ *versus* control. *C* and *D* show similar changes in mRNA (*C*) and protein (*D*) levels after treatment of *in vitro* activated primary HSCs with MDI. The *table* in *D* summarizes densitometric changes in the Western blots. Results are from two HSC preparations done in duplicate. *, $p < 0.05$, and **, $p < 0.005$ *versus* control.

were unchanged in HSCs isolated from BDL rats, nuclear binding activity fell slightly (Fig. 4*C*). Both c-Maf and MafG exhibited increased nuclear binding activity to ARE (Fig. 4*C*). Conversely, following MDI treatment, both c-Maf and MafG nuclear binding activity to ARE fell more than 50%, but Nrf2 binding was unchanged (Fig. 4*D*).

Effects of Maf Knockdown on BSC Activation Status and GCLC Expression—In BDL livers and Huh-7 cells treated with the toxic bile acid lithocholic acid, knockdown of c-Maf and MafG prevented displacement of Nrf2 from ARE and the fall in GCLC expression (7). To see if the same is true in HSCs, activated BSCs were treated with MafG or c-Maf siRNAs, but in contrast to whole liver or lithocholic acid-treated Huh-7 cells, knockdown of MafG in activated BSCs lowered GCLC expression (Fig. 5, *A* and *B*), although c-Maf knockdown had no influence on GCLC expression (data not shown). Knockdown of MafG in activated BSCs resulted in lower Nrf2 binding to the distal GCLC ARE, and SeqChIP assay showed reduced MafG co-occupancy of the same region (Fig. 5*C*), supporting an activator role of Nrf2/MafG heterodimer in ARE-dependent GCLC expression in activated BSCs.

Nrf2/MafG Heterodimerization and Co-occupancy of ARE Region Increased in Quiescent HSCs and Fell in Activated HSCs—Following MDI treatment, interaction between Nrf2 and MafG is markedly enhanced (77-fold) despite 90% reduction in nuclear MafG levels (Fig. 6*A*). Co-occupancy of Nrf2 and MafG to the GCLC distal ARE is increased after MDI treatment (Fig. 6*B*) and falls by 50% in activated HSCs (Fig. 6*C*).

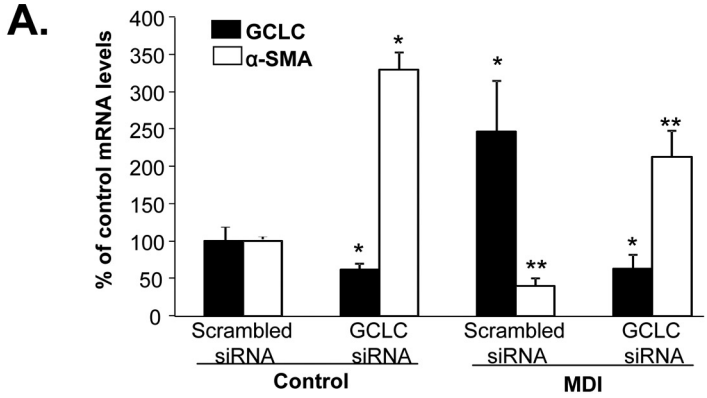

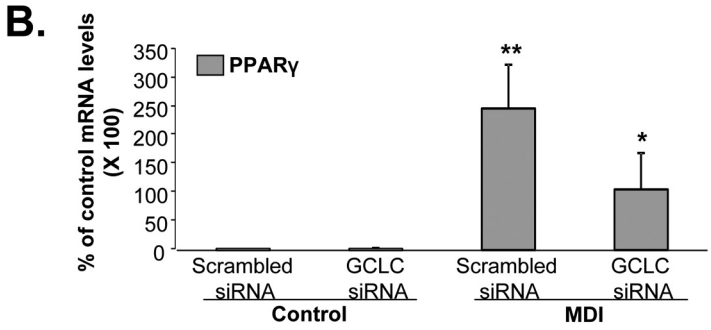

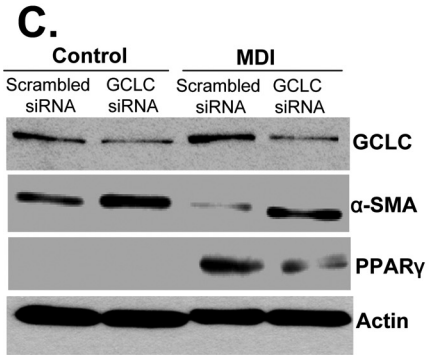

Densitometric ratios over actin
(% of control with scrambled siRNA)

	Scrambled siRNA	GCLC siRNA	MDI+ scrambled siRNA	MDI+ GCLC siRNA
GCLC	100 ± 25.4	**37.5 ± 6.8	*243.8 ± 53	*23.5 ± 9.5
α-SMA	100 ± 5.7	*170.3 ± 27.0	**13.2 ± 4.8	*199.7 ± 36.4
PPARγ	100 ± 15	143 ± 56	**1000 ± 255	*579 ± 213

FIGURE 3. **Reducing GCLC expression keeps HSCs in activated state.** BSCs (control and MDI-treated) were treated with GCLC siRNA or scrambled siRNA to lower the mRNA level by 50%, and the effects on α-SMA and PPARγ at the mRNA (*A* and *B*) and protein (*C*) levels were examined by real time PCR and Western blotting, respectively. The *table* in *C* summarizes densitometric changes in the Western blots. Results are from four experiments done in duplicate for both mRNA and protein levels. *, $p < 0.05$. and **, $p < 0.005$ *versus* control with scrambled siRNA.

Role of SUMO-1 Sumoylation of Nrf2 and MafG in Nrf2/MafG Heterodimerization and GCLC Expression—Protein sumoylation is known to enhance protein/protein interactions (15). Both Nrf2 and MafG contain potential sumoylation sites (supplemental Fig. 1). Fig. 7, *A* and *C*, shows that both MafG and Nrf2 are sumoylated by SUMO-1 in activated BSCs, and this is increased following MDI treatment but only in the nuclear fraction. Although both Nrf2 and MafG are also sumoylated by SUMO-2/3, MDI treatment had no effect on their levels (Fig. 7*B*). Conversely, during HSC activation, sumoylation of Nrf2 and MafG by SUMO-1 falls despite increased nuclear MafG levels (Nrf2 nuclear level was unchanged) (Fig. 7*D*). To evaluate whether this sumoylation is important for Nrf2/MafG interaction and activation of ARE-dependent genes, quiescent BSCs (after 3 days of MDI treatment) were treated with scrambled siRNA or SUMO-1 siRNA for 24 h. SUMO-1 knockdown reduced GCLC expression by about 40–45% (Fig. 8*A*) and interaction between Nrf2 and MafG (Fig. 8*B*) and co-occupancy of the distal ARE region of GCLC (Fig. 8*C*). SUMO-1 knockdown also reduced Nrf2 binding to the ARE, but MafG binding was unaffected (Fig. 8*C*). Following SUMO-1 knockdown, GSH levels fell from 53.98 ± 0.29 to 22.29 ± 2.42 nmol/mg protein (results are mean ± S.E. from three independent experiments, $p < 0.05$).

Identifying Sites of Sumoylation on Nrf2 and MafG—To examine the effect of sumoylation site mutations on the heterodimerization between Nrf2 and MafG, Nrf2 sumoylation site mutant and wild type proteins were overexpressed in BSC cells and tested for their ability to immunoprecipitate MafG. As shown in Fig. 9*A*, control BSC cells expressing an empty vector had low levels of Nrf2-MafG complexes. Overexpression of wild type Nrf2 significantly raised the level of immunoprecipitated MafG, whereas mutant Nrf2 immunoprecipitated even less MafG than empty vector control. Although overexpression of wild type and mutant MafG raised MafG protein levels (Fig. 9*B*), we were not able to see any Nrf2 on Western blot following

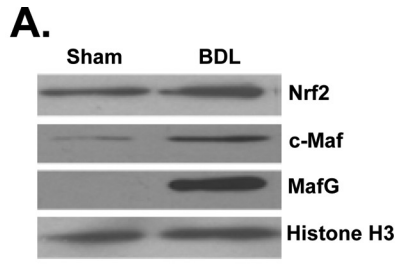

Densitometric ratios over Histone H3 (% of Sham)

	Control	MDI
Nrf2	100 ± 8.2	110.8 ± 12.0
c-Maf	100 ± 4.1	*304.6 ± 32.3
MafG	100 ± 7.2	*910.5 ± 141.2

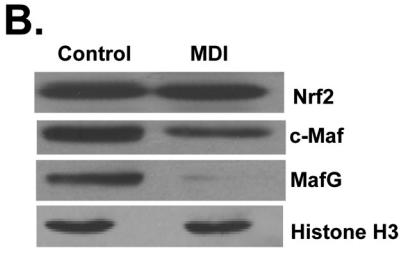

Densitometric ratios over Histone H3 (% of control)

	Control	MDI
Nrf2	100 ± 1.1	121.0 ± 18.4
c-Maf	100 ± 7.1	**46.0 ± 7.1
MafG	100 ± 1.4	*8.0 ± 1.4

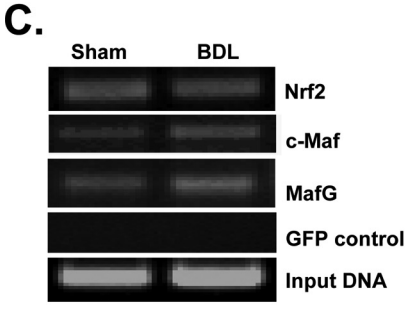

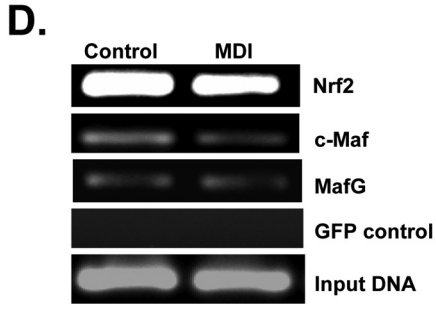

Densitometric ratios over input DNA (% of Sham)

	Sham	BDL
Nrf2	100 ± 4.2	*87 ± 5.1
c-Maf	100 ± 22	**168.3 ± 14.4
MafG	100 ± 32.7	*159.5 ± 24.7

Densitometric ratios over input DNA (% of control)

	Control	MDI
Nrf2	100 ± 23	93.1 ± 11.3
c-Maf	100 ± 33.6	*40.1 ± 13.9
MafG	100 ± 14	**47.9 ± 8.3

FIGURE 4. **Nuclear levels and ARE binding activity of Nrf2, c-Maf, and MafG in activated and quiescent HSCs.** *A* shows nuclear levels of these transcription factors in *in vivo* activated HSCs isolated from 10-day-old BDL livers. The *table* adjacent to blots summarizes densitometric changes from 2 to 3 preparations done in duplicate. *, $p < 0.05$ *versus* sham control. *B* shows nuclear levels of the same transcription factors following MDI treatment of BSCs, and densitometric changes are summarized in the *table* next to the blots. Results are from two experiments done in duplicate. *, $p < 0.005$; **, $p < 0.05$ *versus* control. *C* and *D* show Nrf2, c-Maf, and MafG binding to the GCLC ARE region using ChIP assay in *in vivo* activated HSCs (*C*) and quiescent HSCs (*D*). The *tables* below summarize densitometric changes from 2 to 3 preparations done in duplicate for *C* and three experiments for *D*. *, $p < 0.05$; **, $p < 0.005$ *versus* respective controls.

immunoprecipitation of MafG (data not shown). The functional effect of these mutants on the expression of GCLC was evaluated in BSC cells. As shown in Fig. 9*B*, overexpression of wild type MafG and Nrf2 up to 3-fold raised GCLC protein levels by 2-fold compared with an empty vector control. Overexpression of the sumoylation site mutant of MafG did not affect GCLC expression compared with empty vector control, and overexpression of the Nrf2 mutant lowered GCLC expression compared with empty vector (Fig. 9*B*, *right panel*).

Sumoylation Does Not Affect Nrf2/c-Myc Interaction or Nrf2 Ubiquitination—c-Myc has been reported to interact with Nrf2 and inhibits its signaling (16). In addition, sumoylation has been reported to interfere with ubiquitination of certain target proteins, and Nrf2 is degraded via the ubiquitin-proteasomal pathway (17). To see if the effect of sumoylation may be due to antagonizing c-Myc interaction with Nrf2 or Nrf2 ubiquitination, BSC cells treated with MDI and SUMO-1 or scrambled siRNA were subjected to immunoprecipitation with anti-Nrf2 and blotted for c-Myc and ubiquitin. Fig. 9, *C* and *D*, shows that SUMO-1 knockdown had no effect on Nrf2/c-Myc interaction or the level of ubiquitinated Nrf2.

Effects of GCLC Knockdown on BDL-induced Liver Injury and Fibrosis and Its Treatments—To see if GCLC expression influences fibrosis *in vivo*, we employed lentiviral expression vector to knock down GCLC at the same time as BDL and then repeated it on days 6 and 10. This regimen achieved transduction efficiency of about 89% at day 14 (7). The efficacy of UDCA and AdoMet was then examined in the setting of GCLC knockdown during BDL for 14 days. Fig. 10*A* shows that GCLC siRNA (GCLCi) was able to further reduce the mRNA level of GCLC (50% lower than BDL + SC). UDCA or AdoMet, which completely prevented BDL-induced lowering of GCLC mRNA level (6), was unable to rescue in the presence of GCLCi, although the combined UDCA and AdoMet had 40% higher GCLC mRNA level than BDL + GCLCi alone. Livers from the BDL + GCLCi-treated mice appear more fibrotic, and consistently, Col1A2

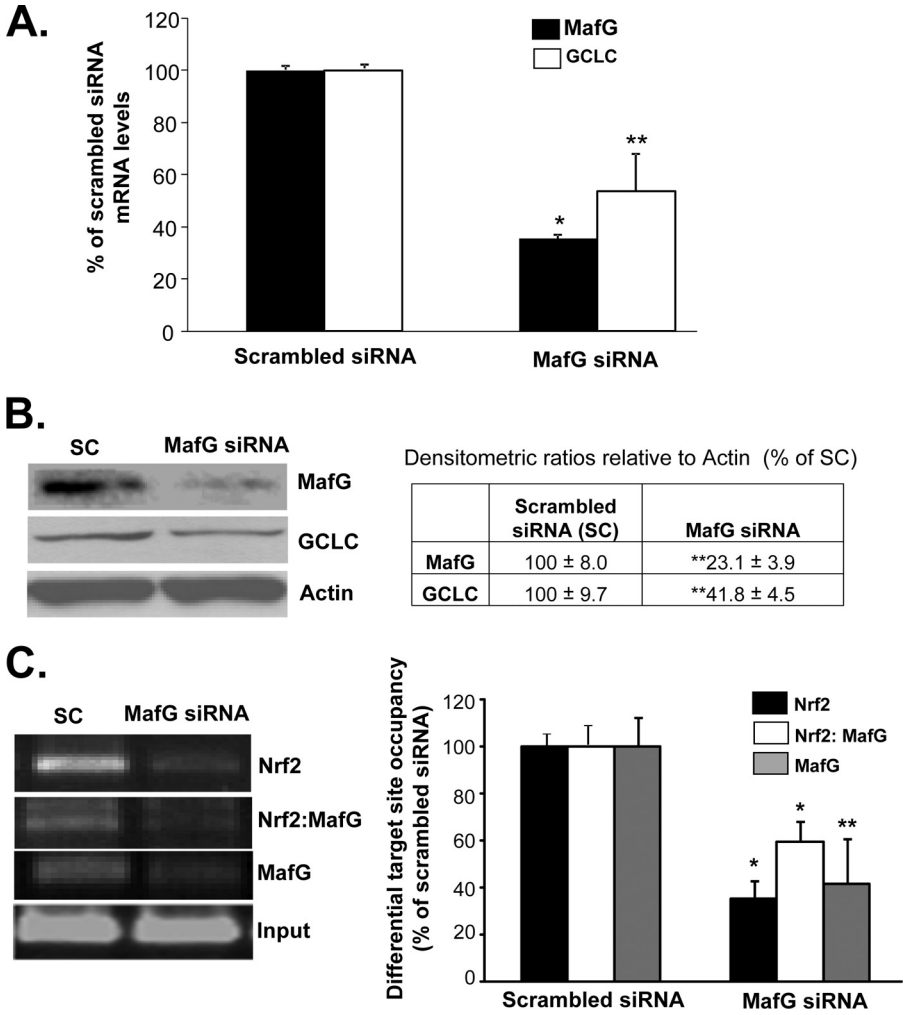

FIGURE 5. **Effect of MafG knockdown on GCLC expression, Nrf2 nuclear binding to ARE, and Nrf2-MafG co-occupancy of the GCLC ARE region in activated BSCs.** BSCs were treated with MafG siRNA, and the effects on GCLC mRNA (*A*) and protein (*B*) levels were measured using real time PCR and Western blotting, respectively. The *table* in *B* summarizes densitometric changes of the Western blots. Results are from two (protein) and three (mRNA) experiments done in duplicate. *, $p < 0.005$; **, $p < 0.05$ *versus* scrambled siRNA. *C* shows nuclear binding activity to the GCLC ARE region of Nrf2, Nrf2-MafG co-occupancy, and MafG following MafG siRNA treatment in BSCs using ChIP and SeqChIP. Densitometric changes are shown in the graph from two experiments done in duplicate. *, $p < 0.005$; **, $p < 0.05$ *versus* scrambled siRNA.

mRNA levels were markedly elevated (5-fold of sham + SC) in the BDL + GCLCi group as compared with the BDL + SC group (2-fold higher than Sham + SC). AdoMet and UDCA had a minimal protective effect against the increase in Col1A2 mRNA levels in the presence of GCLCi, but the levels were still higher than the BDL + SC group. This is also consistent with the quantitative Sirus Red scoring (Table 1). Fig. 10*B* shows marked increase in necrosis, apoptosis, and fibrosis in the GCLCi livers, regardless of whether they received UDCA and/or AdoMet. Table 1 summarizes histological changes and biochemical parameters and liver GSH levels. Consistent with more necrotic foci, ALT levels were significantly higher in BDL + GCLCi group and UDCA and AdoMet failed to exert any protective effect. This is different from the effect of UDCA and AdoMet when they are able to induce GCLC. UDCA and AdoMet lowered ALT levels significantly in BDL mice treated with scrambled siRNA. GCLC knockdown did not alter either the alkaline phosphatase or bilirubin levels, but UDCA and AdoMet failed to exert any protective effect, although they were protective against the rise in bilirubin level when treated with scrambled siRNA (Table 1). Hepatic GSH levels fell by 50% in the BDL group, but this was prevented by either UDCA or AdoMet (and more with both) in scrambled siRNA groups. GSH levels fell by 80% in BDL mice that received GCLCi, and although UDCA and AdoMet were able to protect partially against this fall, the level remained much lower than the respective scrambled siRNA groups (Table 1). Finally, UDCA and AdoMet were able to protect against necrosis, apoptosis, and fibrosis much more effectively in the scrambled siRNA groups as compared with GCLCi groups.

DISCUSSION

GSH is a key antioxidant that is synthesized in all mammalian cells (1). A key factor that regulates the biosynthesis of GSH is the activity of the rate-limiting enzyme GCL, which in turn is regulated dominantly at the transcriptional level (1). Recently, we reported that during prolonged BDL-induced cholestatic liver injury in mice, the expression of GSH synthetic enzymes fell, and this was associated with reduced Nrf2 binding to the ARE and a nearly 4-fold induction of c-Maf and MafG expres-

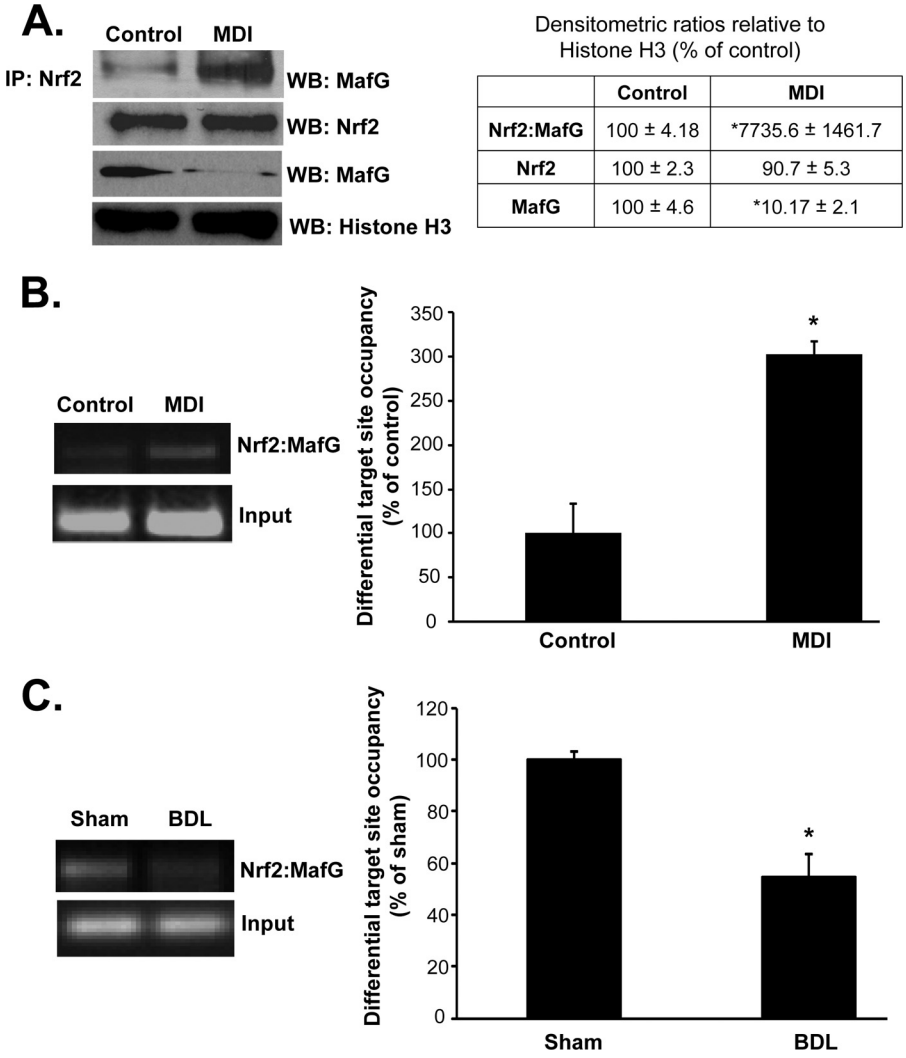

	Control	MDI
Nrf2:MafG	100 ± 4.18	*7735.6 ± 1461.7
Nrf2	100 ± 2.3	90.7 ± 5.3
MafG	100 ± 4.6	*10.17 ± 2.1

FIGURE 6. **Nrf2/MafG interaction and co-occupancy of GCLC ARE region in activated and quiescent HSCs.** *A* shows interaction of Nrf2 with MafG using anti-Nrf2 antibody in co-immunoprecipitation (*IP*) experiment followed by Western blotting (*WB*) for MafG is enhanced following MDI treatment of BSCs despite marked reduction in nuclear MafG levels (nuclear Nrf2 level is unchanged). Densitometric changes are summarized in the adjacent box, and results are from two experiments done in duplicate. *, $p < 0.005$ *versus* control. *B* shows Nrf2-MafG co-occupancy of the GCLC ARE region using SeqChIP is enhanced following MDI treatment of BSCs but falls by nearly 50% in *in vivo* activated HSCs (*C*). Densitometric changes are summarized in adjacent *graphs*, and results are from three experiments each for *B* and *C* done in duplicate. *, $p < 0.005$ *versus* respective controls.

sion and binding to the ARE (6, 7). ARE is a *cis*-acting regulatory element found in the 5′-regulatory region of almost all of the enzymes involved in phase II metabolism of xenobiotics that include GCL, quinone reductase, glutathione *S*-transferase, and epoxide hydrolase, which play important roles in defense against oxidative stress and toxins (18, 19). Nrf2 is a member of the cap 'n' collar-basic leucine zipper proteins that *trans*-activates ARE (19). Under nonstressful conditions, Nrf2 is kept in the cytosol by Keap1 and undergoes proteasomal degradation (20). Upon recognition of stressful signals, Nrf2 is released from Keap1, escapes proteasomal degradation, and translocates to the nucleus to induce genes involved in defense and survival (20). Nrf2 forms heterodimers with small Maf (MafG, MafK, and MafF) and Jun (c-Jun, Jun-D, and Jun-B) proteins to bind to ARE (19). Nrf2/MafG heterodimer generally activates ARE-dependent gene transcription and has also been reported to enhance Nrf2 nuclear retention (19, 21). However, the small Mafs can form homodimers or heterodimerize with c-Maf to repress ARE-mediated gene expression (22, 23). We speculated that in the setting of prolonged BDL, displacement of Nrf2 from ARE may have resulted from enhanced MafG/MafG homodimer and/or c-Maf/MafG heterodimer binding to the ARE to result in lower GCL expression. This is supported by the observation that blocking c-Maf and MafG induction during BDL prevented the fall in GCL expression and BDL-induced liver injury, including fibrosis (7).

Accumulating evidence show the importance of GSH as a regulator of the fibrogenic response in HSCs. Oxidative stress is known to activate HSCs, and several agents that exert antifibrotic effects all elevate GSH levels (3–5). Our work in BDL mice also showed prevention of the fall in GSH ameliorated against liver injury and fibrosis (7). Despite these reports, changes in GSH synthesis during fibrogenesis is poorly characterized, and whether they play a causative role or are secondary effects are not known. This study was aimed at improving our understanding of the role of GSH in HSC phenotypes. To this

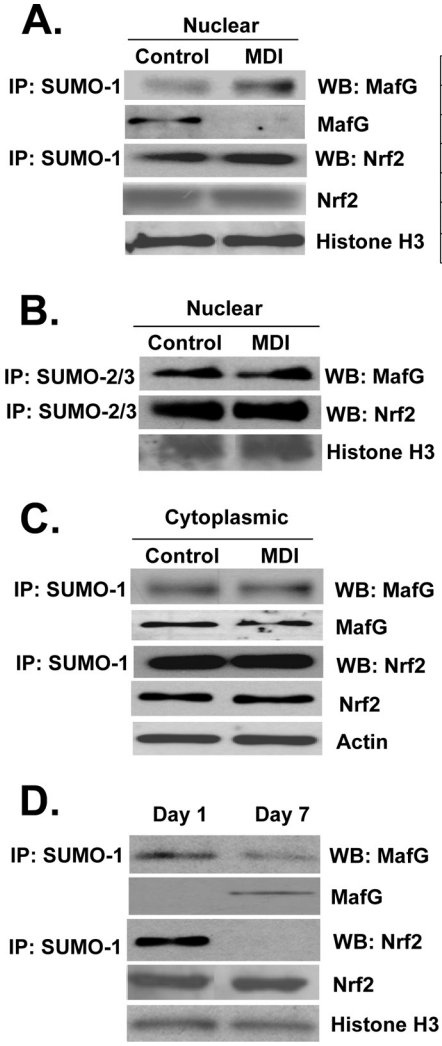

Densitometric ratios relative to Histone H3 (% of control)

Nuclear	Control	MDI
IP SUMO-1:MafG	100 ± 7.5	*310 ± 77.4
MafG	100 ± 5.0	*14.3 ± 1.7
IP SUMO-1:Nrf2	100 ± 2.3	*250.1 ± 34.2
Nrf2	100 ± 34.2	90.5 ± 11.2
Sumoylated MafG/MafG	100 ± 31.2	*2151 ± 537
Sumoylated Nrf2/Nrf2	100 ± 2.1	*300 ± 40.9

Densitometric ratios relative to Actin (% of control)

Nuclear	Control	MDI
IP SUMO-2/3:MafG	100 ± 18.8	116.3 ± 5.1
IP SUMO-2/3:Nrf2	100 ± 17.9	102.4 ± 9.8

Densitometric ratios relative to Actin (% of control)

Cytoplasmic	Control	MDI
IP SUMO-1:MafG	100 ± 5.6	79.3 ± 13.5
MafG	100 ± 7.6	95.8 ± 29.1
IP SUMO-1:Nrf2	100 ± 10.9	103.9 ± 25.2
Nrf2	100 ± 3.8	88.5 ± 5.5

Densitometric ratios relative to Histone H3 (% of Day 1)

	Day 1	Day 7
IP SUMO-1:MafG	100 ± 35.6	*51.4 ± 9.9
MafG	100 ± 1.35	*820.0 ± 250.1
IP SUMO-1:Nrf2	100 ± 0.01	**10.5 ± 0.1
Nrf2	100 ± 6.7	110.9 ± 11.7

FIGURE 7. **Changes in MafG and Nrf2 sumoylation in quiescent and activated HSCs.** *A,* MDI treatment of BSCs increased SUMO-1 sumoylation of MafG and Nrf2 in the nuclear fraction despite marked reduction in nuclear MafG level. Results are from 3 to 4 experiments done in duplicate. *, $p < 0.005$ *versus* control. *B,* MDI treatment of BSC cells does not change SUMO-2/3-mediated sumoylation of MafG or Nrf2 in the nuclear fraction. *C,* same experiment as in *A* showing MDI treatment of BSCs did not alter cytoplasmic sumoylated and total MafG or Nrf2 levels. *D,* activation of primary HSCs in culture decreased nuclear level of SUMO-1 sumoylation of Nrf2 and MafG. Results are from two HSC preparations in duplicate. *, $p < 0.05$; **, $p < 0.005$ *versus* day 1 HSCs. Densitometric changes are summarized in adjacent *tables*. *IP*, immunoprecipitation; *WB*, Western blot.

end, we studied both HSC activation and reversion back to quiescence using MDI, a well described treatment regimen (11). We found that during *in vitro* activation of HSCs, the expression of both GCL subunits and GS fell at the mRNA level, but only GCLC was suppressed at both mRNA and protein levels in *in vivo* activated HSCs (Fig. 1). Differences in *in vitro* and *in vivo* activation of HSCs are well described (24). Despite the well documented importance of GCLM in GCL activity, we found no change in GCLM protein level during HSC activation. This has also been reported by other investigators, specifically treatment of HSCs by TGF-β1 lowered GCLC expression without affecting GCLM (4) and treatment with epigallocatechin-3-gallate, which inhibits HSC activation, also induced GCLC expression without changing GCLM (4). GSH levels fell in parallel to the GCLC protein levels. Taken together, these results suggest GCLC is limiting in HSCs.

Because GCLC was down-regulated in both models and at the protein level in *in vivo* activated HSCs, we focused our effort on elucidating the mechanism and significance. Consistent with an important role of GCLC expression in determining the HSC phenotype, reversion of activated HSCs (both BSCs and *in vitro* activated primary HSCs) back to quiescence required activation of GCLC expression as blocking its induction kept HSCs in an activated state (Figs. 2 and 3). Interestingly, HSCs obtained from sham-operated rats contain both 73-kDa bands and the cleaved 60-kDa GCLC bands (Fig. 1*E*). The 60-kDa band is known to be induced during apoptosis in HeLa and Jurkat cells (25). Its presence in HSCs has not been shown previously. During isolation of HSCs, cells are treated with detergents and enzymes, which may have triggered cleavage of GCLC. Because HSCs from BDL rats have a nearly 60% fall in the 73-kDa band, although the 60-kDa band is unchanged, the ratio of the 73:60-kDa bands fell suggesting that increased cleavage may have also contributed to the fall in active GCLC during HSC activation.

Similar to what we observed in BDL livers, activated HSCs have increased nuclear levels of c-Maf and MafG and binding to ARE, whereas the opposite occurred in quiescent HSCs (Fig. 4). However, Nrf2 binding to ARE was minimally affected, which is

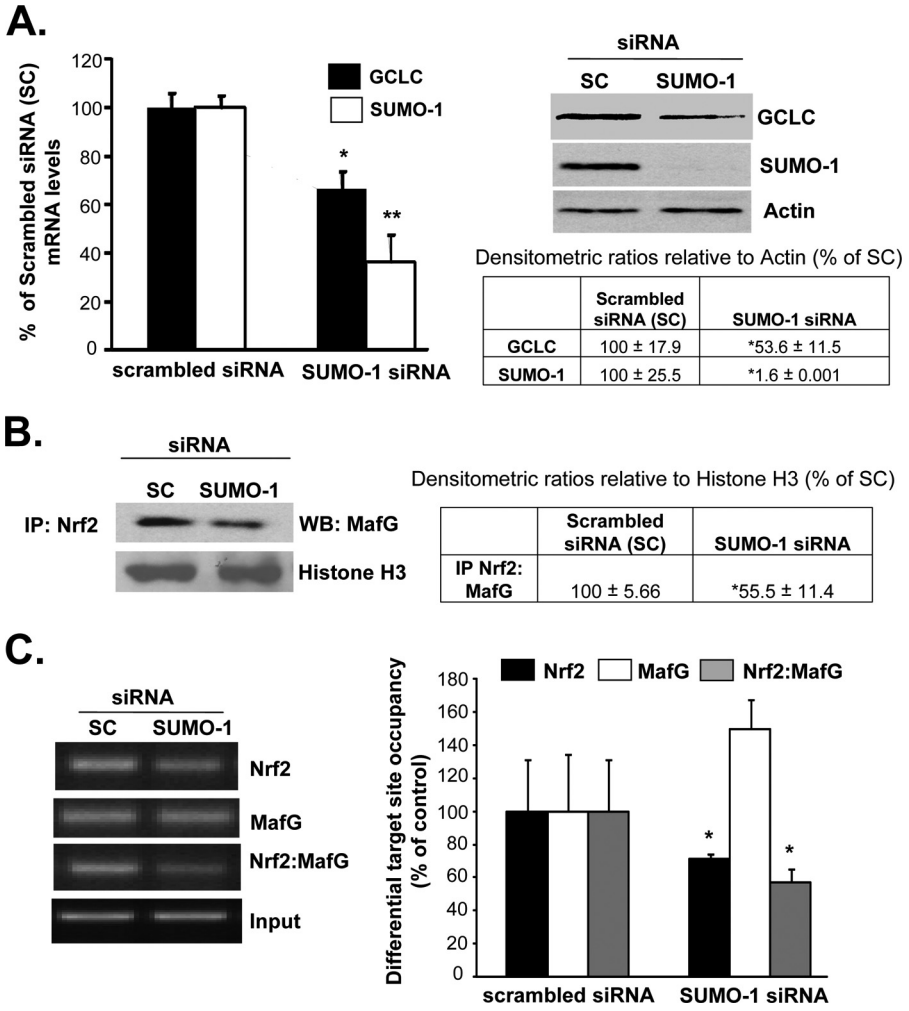

FIGURE 8. **SUMO-1-mediated sumoylation is required for Nrf2/MafG interaction, ARE binding, and GCLC expression.** *A* shows effect of SUMO-1 knockdown on GCLC mRNA and protein levels in MDI-treated BSCs. Densitometric changes are summarized in the *box* below the Western blots (*WB*). Results are from three experiments done in duplicate. *, $p < 0.005$ *versus* scrambled siRNA. *B* shows SUMO-1 knockdown reduced interaction between Nrf2 and MafG in co-immunoprecipitation (*IP*) experiments. Densitometric changes are shown in *adjacent box*, and results are from three experiments done in duplicate. *, $p < 0.005$ *versus* scrambled siRNA. *C* shows SUMO-1 knockdown lowered Nrf2 binding and Nrf2-MafG co-occupancy to the GCLC ARE region. Densitometric changes are summarized in the adjacent *graph*, and results are from three experiments done in duplicate. *, $p < 0.005$ *versus* scrambled siRNA.

different from BDL livers (6, 7). In addition, GCLC expression increased when MafG or c-Maf induction was prevented in BDL livers (7), but in activated HSCs, knocking down c-Maf had no effect on GCLC expression, and knocking down MafG lowered GCLC expression further (Fig. 5). Reducing MafG expression in activated HSCs reduced Nrf2 binding to the ARE and heterodimerization of Nrf2 with MafG (Fig. 5), whereas enhanced heterodimerization of Nrf2 with MafG occurred in quiescent HSCs (Fig. 6). The most perplexing part was that in quiescent HSCs, enhanced heterodimerization of Nrf2 and MafG occurred despite 90% reduction in nuclear MafG levels, whereas in activated HSCs, reduced heterodimerization occurred despite a marked increase in nuclear MafG levels. The most likely explanation was that either critical post-translational modification was altering their interaction or unknown co-factor(s) were involved that affected their heterodimerization.

Nrf2 is regulated post-translationally (26). For instance, PKC phosphorylates Nrf2 at serine 40 to result in the escape of Nrf2 from Keap1 for translocation to the nucleus, and Fyn phosphorylates Nrf2 at tyrosine 568 to result in nuclear export of Nrf2 (26). However, there is no report of post-translational modification of Nrf2 that affects its interaction with MafG or DNA binding. Sumoylation is known to affect protein/protein interactions, and interestingly, MafG has been reported to be sumoylated by SUMO-2 and -3 (27). In bone marrow cells, sumoylated MafG exerts a repressive effect (27). Of the three potential sumoylation sites in MafG, two are in the bZIP domain, which heterodimerizes with Nrf2, and one is in the N-terminal domain outside of the bZIP region (supplemental Fig. 1). Nrf2 also has two potential sumoylation sites in the bZIP domain, which is essential for heterodimerization with MafG (supplemental Fig. 1) (21), but whether Nrf2 is sumoylated and how sumoylation affects Nrf2 function have not been reported. We investigated whether Nrf2 and MafG might be sumoylated by SUMO-1 as a PPARγ has been reported to be sumoylated by SUMO-1 (28). We found that both Nrf2 and MafG are indeed sumoylated by SUMO-1 in HSCs and sumoylated Nrf2 and MafG nuclear levels are higher in quiescent HSCs as compared with activated HSCs (Fig. 7). Interestingly, in quiescent HSCs,

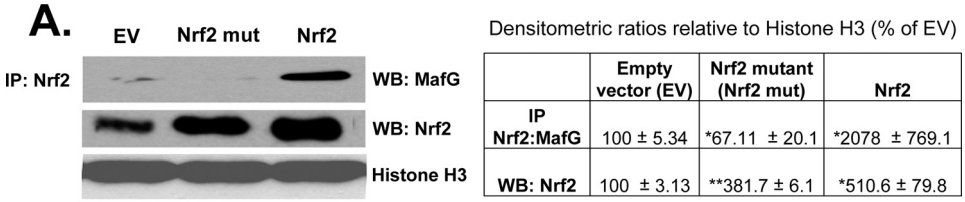

Densitometric ratios relative to Histone H3 (% of EV)

	Empty vector (EV)	Nrf2 mutant (Nrf2 mut)	Nrf2
IP Nrf2:MafG	100 ± 5.34	*67.11 ± 20.1	*2078 ± 769.1
WB: Nrf2	100 ± 3.13	**381.7 ± 6.1	*510.6 ± 79.8

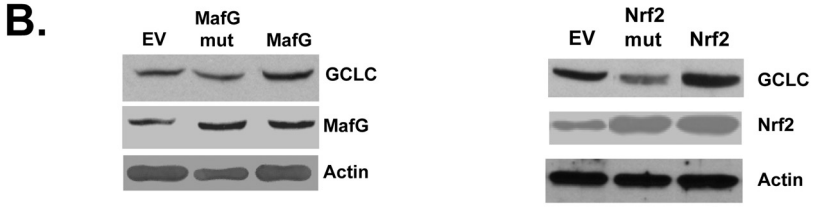

Densitometric ratios relative to Actin (% of EV)

	EV	MafG mutant (MafG mut)	MafG
GCLC	100 ± 3.6	96.5 ± 19.2	*275.6 ± 70.4
MafG	100 ± 1.9	*233.5 ± 31.7	*289.8 ± 57.2

	EV	Nrf2 mutant (Nrf2 mut)	Nrf2
GCLC	100 ± 5.7	*66.8 ± 10.7	**255.4 ± 2.8
Nrf2	100 ± 3.1	**321.9 ± 6.1	*418.1 ± 79.8

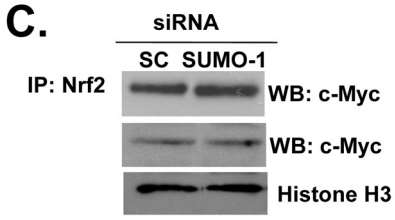

Densitometric ratios relative to Actin (% of SC)

	Scrambled siRNA (SC)	SUMO-1 siRNA
IP Nrf2: c-Myc	100 ± 47.6	183.8 ± 81.2
c-Myc	100 ± 9.1	93 ± 5.4

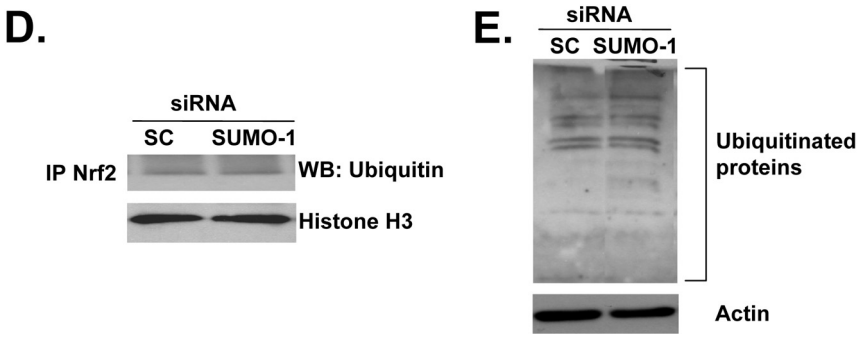

FIGURE 9. **SUMO-1 sumoylation of Nrf2 and MafG at specific sites affect their interaction and GCLC expression but not Nrf2/c-Myc interaction or Nrf2 ubiquitination.** *A,* effect of mutating the SUMO-1 sites on Nrf2 and MafG (see supplemental Fig. 1) on Nrf2/MafG interaction in HSCs. Sumoylation site mutants of Nrf2 and MafG were overexpressed in BSC cells along with their corresponding normal constructs. Nuclear extracts of these cells were immunoprecipitated (*IP*) with Nrf2 and checked for MafG expression by Western blotting (*WB*). Results are from two experiments in duplicate. *, $p < 0.05$; **, $p < 0.005$ *versus* empty vector control. *B,* mutant and wild type constructs were expressed as in *A,* and the expression of GCLC was examined by Western blotting. Results are from three experiments in duplicate. *, $p < 0.05$; **, $p < 0.005$ *versus* empty vector control. *C* and *D,* effect of SUMO-1 knockdown on interaction of Nrf2 with c-Myc protein and ubiquitin. Nuclei from MDI BSC cells were treated with scrambled (*SC*) or SUMO-1 siRNA, and nuclear extracts were processed for immunoprecipitation of Nrf2 followed by Western blotting for c-Myc (*C*) or ubiquitin (*D*). Results are from two experiments in duplicate. *E,* effect of SUMO-1 knockdown on total ubiquitinated proteins in MDI-treated BSC cells. Total protein extracts from scrambled (*SC*) or SUMO-1 siRNA cells were subjected to Western blotting using anti-ubiquitin antibody. Results are from two experiments in duplicate.

despite a nearly 90% reduction in nuclear MafG, the ratio of sumoylated MafG to total MafG increased 20-fold. The opposite was true in activated HSCs. A critical role of SUMO-1 in facilitating the Nrf2/MafG interaction and ARE binding is demonstrated by knocking down SUMO-1 in quiescent HSCs, which resulted in reduced Nrf2 binding to the ARE and heterodimerization with MafG. Sumoylation did not alter MafG binding to the ARE, but as Nrf2/MafG heterodimer binding was reduced, GCLC expression fell by 50%, and GSH levels fell nearly 60%. We were not able to evaluate SUMO-1 knockdown in activated HSCs as SUMO-1 siRNA treatment in activated HSCs resulted in significant cell death in less than 24 h (results not shown), but this did not occur if they were treated with MDI. We also found that Nrf2 and MafG are sumoylated by SUMO-2/3 in HSC, but their levels were unaffected by a change in the HSC phenotype. It has been shown that treatment of RAW cells with low doses of hydrogen peroxide inhibited SUMO-1 conjugating activity, and this can be reversed by treatment with reduced GSH (29). This together with our findings suggest an interesting scenario where oxidative stress that occurs during HSC activation could inhibit SUMO-1 conjugation of Nrf2 and MafG to impair their interaction leading to

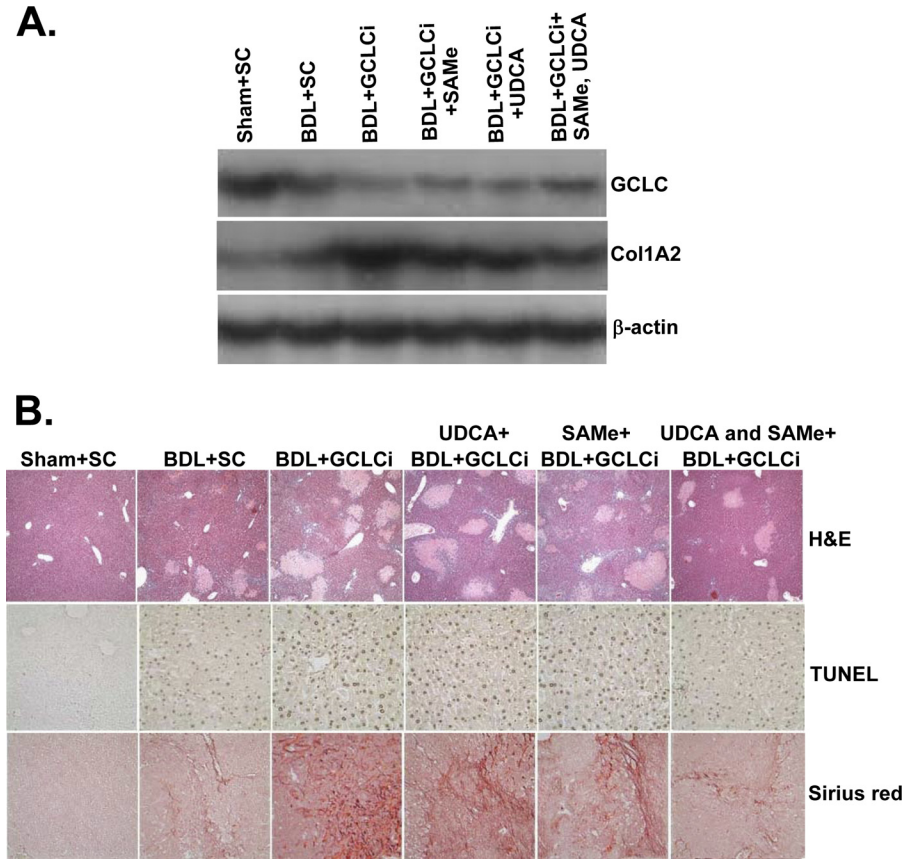

FIGURE 10. **Effects of GCLC siRNA on hepatic GCLC and Col1A2 mRNA levels and histopathology in BDL mice treated with UDCA and/or AdoMet.** Mice were treated with BDL or sham surgery, with or without scrambled or GCLC siRNA (GCLCi) delivered at days 0, 6, and 10, and UDCA ± AdoMet (both 100 mg/kg/day by gavage) for 14 days. *A* shows mRNA levels determined in the livers at day 14 using Northern blot analysis. Representative from $n = 4$ mice per group is shown. *B* shows H&E, TUNEL, and Sirus Red stains from representative livers. Quantitative scores are shown in Table 1.

TABLE 1

Effect of GCLC knockdown on BDL liver injury and treatment efficacy after 14 days

Results are mean ± S.E. from four to eight mice for each group. Mice were treated with GCLC or scrambled siRNA and BDL or sham surgery. UDCA and AdoMet were administered by gavage at 100 mg/kg/day in a 0.1-ml volume.

	ALT	Alkaline phosphatase	Bilirubin	Liver GSH	Necrosis	Apoptosis	Sirius Red
	units/liter	*units/liter*	*μmol/liter*	*nmol/mg protein*	*% total*	*% total*	*% total*
Scrambled siRNA +							
Sham	37 ± 2	96 ± 5	16 ± 5	44.0 ± 1.8	0 ± 0	0.8 ± 0.1	0.6 ± 0.1
BDL	728 ± 41[a]	568 ± 52[a]	302 ± 18[aa]	22.4 ± 3.7[a]	26 ± 2[a]	20.7 ± 2.0[a]	6.8 ± 0.7[a]
BDL + UDCA	326 ± 65[a,b]	462 ± 83[a]	217 ± 31[a,b]	51.8 ± 1.1[a,b]	20 ± 2[a]	13.2 ± 2.1[a,b]	4.6 ± 0.5[a]
BDL + AdoMet	348 ± 52[a,b]	551 ± 86[a]	202 ± 30[a,b]	49.8 ± 3.6[b]	21 ± 2[a]	16.9 ± 1.6[a,b]	5.2 ± 0.2[a]
BDL + UDCA, AdoMet	356 ± 16[a,b]	641 ± 36[a]	196 ± 24[a,b]	58.8 ± 2.9[a,b]	18 ± 3[a,b]	11.8 ± 1.6[a,b]	3.8 ± 0.4[a,b]
GCLC siRNA +							
BDL	933 ± 67[a,b]	678 ± 48[a]	330 ± 47[a]	8.4 ± 2.6[a,b]	36 ± 2[a,b]	36.5 ± 2.6[a,b]	15.0 ± 1.6[a,b]
BDL + UDCA	983 ± 41[a,b,c]	711 ± 39[a,c]	261 ± 52[a]	18.0 ± 2.2[a,c,d]	29 ± 2[a,c]	31.9 ± 0.9[a,b,c]	13.7 ± 2.1[a,b,c]
BDL + AdoMet	970 ± 20[a,b,c]	661 ± 51[a]	250 ± 49[a]	15.4 ± 1.9[a,c,d]	30 ± 3[a]	32.3 ± 2.4[a,b,c]	14.2 ± 1.3[a,b,c]
BDL + UDCA, AdoMet	827 ± 77[a,c]	616 ± 39[a]	241 ± 54[a]	28.1 ± 2.3[a,c,d]	27 ± 2[a,d]	23.0 ± 2.4[a,c,d]	10.6 ± 1.1[a,b,c]

[a] $p < 0.001$ *versus* sham + scrambled siRNA.
[b] $p < 0.05$ *versus* BDL + scrambled siRNA.
[c] $p < 0.05$ *versus* BDL + scrambled siRNA and UDCA, AdoMet, or both.
[d] $p < 0.05$ *versus* BDL + GCLC siRNA.

down-regulation of GCLC expression and lowering of the GSH level, which can further perpetuate the fibrogenic process. We have identified site(s) of sumoylation on both Nrf2 and MafG. Mutation analysis of these sites shows that intact Nrf2 sumoylation sites are required for its interaction with MafG in BSC cells. Mutations of the MafG or Nrf2 sumoylation sites abrogated their positive regulatory effect on GCLC expression. The effect of sumoylation is not due to inhibiting the Nrf2/cMyc interaction or Nrf2 ubiquitination. Overexpression of the Nrf2 mutant lowered GCLC expression compared with the empty vector, indicating that the Nrf2 sumoylation mutant may have a dominant negative effect on GCLC expression. Taken together, these results show that the critical factor that determined Nrf2/MafG heterodimerization and subsequent ARE binding and GCLC expression in HSCs is SUMO-1-mediated sumoylation of these transcription factors.

The results in HSCs appear to differ from that of the BDL livers (7). There are multiple possible explanations. The models

and cell types are different. In the BDL study, preventing the induction of MafG and c-Maf largely in hepatocytes protected against the BDL-induced fall in GCLC expression, liver injury, and fibrosis. In this study, knocking down MafG (but not c-Maf) expression in activated HSCs lowered the already reduced Nrf2/MafG heterodimerization and GCLC expression. This would suggest that there is a cell type-specific regulation of these transcription factors and/or their post-translational modifications in how they affect ARE-mediated gene expression. In the BDL situation, protecting hepatocyte cell death likely was the main factor that ameliorated against liver fibrosis.

Finally, we addressed the question of whether GCLC is an important determinant in BDL-induced liver injury, fibrosis, and a target of therapeutic agents like UDCA and AdoMet. Our results show that lower GCLC expression sensitizes the liver to cholestatic liver injury and accelerates the fibrotic process. They also support the notion that GCLC expression (and GSH level) is a critical element in the cytoprotective action of UDCA and/or AdoMet. This has important clinical implication as hepatic GCLC expression is lower in several human conditions, including diabetes mellitus, alcoholic liver disease, and aging (3). This result contrasts with the report from Haque *et al.* (30) that mice deficient in *Gclm* (with low liver GSH levels) exhibited attenuated progression of diet-induced steatohepatitis and progression to fibrosis. However, the investigators found that genetic deletion of *Gclm* in mice resulted in compensatory adaptation to low GSH with heightened antioxidant capacity and handling of endogenous and exogenous compounds (30). Because we employed acute knockdown with siRNA, compensatory mechanisms are not involved, and under these circumstances an important role of GCLC and GSH was clearly shown.

In conclusion, we have demonstrated an important role of GCLC expression as a determinant of the HSC phenotype. GCLC expression and GSH levels are higher in quiescent HSCs and they fall during activation. The mechanism involves changes in SUMO-1-mediated sumoylation of Nrf2 and MafG, which is an important factor that modulates their interaction and binding to ARE to activate ARE-dependent genes such as GCLC. This has not been previously reported to our knowledge. In addition, we have shown an important role of GCLC expression in BDL-induced liver injury and fibrosis and that its induction is required for UDCA and AdoMet to exert their full therapeutic effects.

Acknowledgments—293T cells and isolated mouse hepatocytes were provided by the Cell Culture Core, and pathological sections and staining were done by the Imaging Core of the University of Southern California Research Center for Liver Diseases (supported by National Institutes of Health Grant P30DK48522). Hepatic stellate cells from sham and BDL rats were provided by the Non-Parenchymal Cell Core of the University of Southern California-UCLA Research Center for Alcoholic Liver and Pancreatic Diseases and Cirrhosis (supported by National Institutes of Health Grant R24 AA12885-07).

REFERENCES

1. Lu, S. C. (2009) Regulation of glutathione synthesis. *Mol. Aspects Med.* **30,** 42–59
2. Burt, A. D. (1993) Cellular and molecular aspects of hepatic fibrosis. *J. Pathol.* **170,** 105–114
3. Iredale, J. P. (2001) Hepatic stellate cell behavior during the resolution of liver injury. *Semin. Liver Dis.* **21,** 427–436
4. Fu, Y., Zheng, S., Lu, S. C., and Chen, A. (2008) Epigallocatechin-3-gallate inhibits growth of activated hepatic stellate cells by enhancing the capacity of glutathione synthesis. *Mol. Pharmacol.* **73,** 1465–1473
5. Zheng, S., Yumei, F., and Chen, A. (2007) Epigallocatechin-3-gallate inhibits growth of activated hepatic stellate cells by enhancing the capacity of glutathione synthesis. *Free Radic. Biol. Med.* **43,** 444–453
6. Yang, H., Ramani, K., Xia, M., Ko, K. S., Li, T. W., Oh, P., Li, J., and Lu, S. C. (2009) Dysregulation of glutathione synthesis during cholestasis in mice. Molecular mechanisms and therapeutic implications. *Hepatology* **49,** 1982–1991
7. Yang, H., Ko, K., Xia, M., Li, T. W., Oh, P., Li, J., and Lu, S. C. (2010) Induction of avian musculoaponeurotic fibrosarcoma proteins by toxic bile acid inhibits expression of GSH synthetic enzymes and contributes to cholestatic liver injury in mice. *Hepatology* **51,** 1291–1301
8. Lu, S. C. (2000) Molecule in focus. *S*-Adenosylmethionine. *Int. J. Biochem. Cell Biol.* **32,** 391–395
9. Tsukamoto, H., Cheng, S., and Blaner, W. S. (1996) Effects of dietary polyunsaturated fat on ethanol-induced Ito cell activation. *Am. J. Physiol.* **270,** G581–G586
10. Sung, C. K., She, H., Xiong, S., and Tsukamoto, H. (2004) Tumor necrosis factor-α inhibits peroxisome proliferator-activated receptor γ activity at a post-translational level in hepatic stellate cells. *Am. J. Physiol.* **286,** G722–G729
11. She, H., Xiong, S., Hazra, S., and Tsukamoto, H. (2005) Adipogenic transcriptional regulation of hepatic stellate cells. *J. Biol. Chem.* **280,** 4959–4967
12. Xia, M., Chen, Y., Wang, L. C., Zandi, E., Yang, H., Bemanian, S., Martínez-Chantar, M. L., Mato, J. M., and Lu, S. C. (2010) Novel function and intracellular localization of methionine adenosyltransferase 2b splicing variants. *J. Biol. Chem.* **285,** 20015–20021
13. Furlan-Magaril, M., Rincón-Arano, H., and Recillas-Targa, F. (2009) Sequential chromatin immunoprecipitation protocol. ChIP-reChIP. *Methods Mol. Biol.* **543,** 253–266
14. Yang, H., Magilnick, N., Ou, X., and Lu, S. C. (2005) Tumor necrosis α induces coordinated activation of rat GSH synthetic enzymes via NFκB and AP-1. *Biochem. J.* **391,** 399–408
15. Müller, S., Hoege, C., Pyrowolakis, G., and Jentsch, S. (2001) SUMO, ubiquitin's mysterious cousin. *Nat. Rev. Mol. Cell Biol.* **2,** 202–210
16. Levy, S., and Forman, H. J. (2010) c-Myc is an Nrf2-interacting protein that negatively regulates phase II genes through their electrophile-responsive elements. *IUBMB Life* **62,** 237–246
17. Stewart, D., Killeen, E., Naquin, R., Alam, S., and Alam, J. (2003) Degradation of transcription factor Nrf2 via the ubiquitin-proteasome pathway and stabilization by cadmium. *J. Biol. Chem.* **278,** 2396–2402
18. Nguyen, T., Huang, H. C., and Pickett, C. B. (2000) Transcriptional regulation of the antioxidant response element. *J. Biol. Chem.* **275,** 15466–15473
19. Jaiswal, A. K. (2004) Nrf2 signaling in coordinated activation of antioxidant gene expression. *Free Radic. Biol. Med.* **36,** 1199–1207
20. Kensler, T. W., Wakabayashi, N., and Biswal, S. (2007) Cell survival responses to environmental stresses via the Keap1-Nrf2-ARE pathway. *Annu. Rev. Pharmacol. Toxicol.* **47,** 89–116
21. Li, W., Yu, S., Liu, T., Kim, J. H., Blank, V., Li, H., and Kong, A. N. (2008) Heterodimerization with small Maf proteins enhances nuclear retention of Nrf2 via masking the NESzip motif. *Biochim. Biophys. Acta* **1783,** 1847–1856
22. Dhakshinamoorthy, S., and Jaiswal, A. K. (2000) Small Maf (MafG and MafK) proteins negatively regulate antioxidant response element-mediated expression and antioxidant induction of the NAD(P)H:quinone oxidoreductase 1 gene. *J. Biol. Chem.* **275,** 40134–40141
23. Dhakshinamoorthy, S., and Jaiswal, A. K. (2002) c-Maf negatively regulates ARE-mediated detoxifying enzyme genes expression and anti-oxidant induction. *Oncogene* **21,** 5301–5312
24. Maubach, G., Lim, M. C., Chen, J., Yang, H., and Zhuo, L. (2011) miRNA studies in *in vitro* and *in vivo* activated hepatic stellate cells. *World J. Gastroenterol.* **17,** 2748–2773

25. Franklin, C. C., Krejsa, C. M., Pierce, R. H., White, C. C., Fausto, N., and Kavanagh, T. J. (2002) Caspase-3-dependent cleavage of the glutamate-L-cysteine ligase catalytic subunit during apoptotic cell death. *Am. J. Pathol.* **160,** 1887–1894
26. Niture, S. K., Kaspar, J. W., Shen, J., and Jaiswal, A. K. (2010) Nrf2 signaling and cell survival. *Toxicol. Appl. Pharmacol.* **244,** 37–42
27. Motohashi, H., Katsuoka, F., Miyoshi, C., Uchimura, Y., Saitoh, H., Francastel, C., Engel, J. D., and Yamamoto, M. (2006) MafG sumoylation is required for active transcriptional repression. *Mol. Cell. Biol.* **26,** 4652–4663
28. Ohshima, T., Koga, H., and Shimotohno, K. (2004) Transcriptional activity of peroxisome proliferator-activated receptor γ is modulated by SUMO-1 modification. *J. Biol. Chem.* **279,** 29551–29557
29. Bossis, G., and Melchior, F. (2006) Regulation of SUMOylation by reversible oxidation of SUMO-conjugating enzymes. *Mol. Cell* **21,** 349–357
30. Haque, J. A., McMahan, R. S., Campbell, J. S., Shimizu-Albergine, M., Wilson, A. M., Botta, D., Bammler, T. K., Beyer, R. P., Montine, T. J., Yeh, M. M., Kavanagh, T. J., and Fausto, N. (2010) Attenuated progression of diet-induced steatohepatitis in glutathione-deficient mice. *Lab. Invest.* **90,** 1704–1717